Classical Cepheid Pulsation Models: IX. New Input Physics

Silvia Petroni

Dipartimento di Fisica, Università degli Studi di Pisa, Via Buonarroti 2, Pisa, 56127 Italy

petroni@df.unipi.it

Giuseppe Bono

INAF-Osservatorio Astronomico di Roma, Via Frascati 33, 00040 Monte Porzio Catone, Italy

bono@mporzio.astro.it

Marcella Marconi

INAF-Osservatorio Astronomico di Capodimonte, Via Moiariello 16, 80131 Napoli, Italy

marcella@na.astro.it

Robert F. Stellingwerf

SC, 2229 Loma Linda, Los Alamos, NM 87544, USA

rfs@stellingwerf.com

ABSTRACT

We constructed several sequences of classical Cepheid envelope models at solar chemical composition ($Y = 0.28, Z = 0.02$) to investigate the dependence of the pulsation properties predicted by linear and nonlinear hydrodynamical models on input physics. To study the dependence on the equation of state (EOS) we performed several numerical experiments by using the simplified analytical EOS originally developed by Stellingwerf and the recent analytical EOS developed by Irwin. Current findings suggest that the pulsation amplitudes as well as the topology of the instability strip marginally depend on the adopted EOS.

To compromise between accuracy and numerical complexity we computed new EOS tables using the Irwin analytical EOS. We found that the difference between analytical and tabular thermodynamic quantities and their derivatives are smaller than 2 % when adopting suitable steps in temperature and density. To improve the numerical accuracy of physical quantities we are now adopting

bicubic splines to interpolate both opacity and EOS tables. The new approach presents the substantial advantage to avoid numerical derivatives both in linear and in nonlinear models. The EOS first and second order derivatives are estimated by means of the analytical EOS or by means of analytical derivatives of the interpolating function. The opacity first order derivatives are evaluated by means of analytical derivatives of the interpolating function.

We also investigated the dependence of observables predicted by theoretical models on the mass-luminosity (ML) relation and on the spatial resolution across the Hydrogen and the Helium partial ionization regions. We found that nonlinear models are marginally affected by these physical and numerical assumptions. In particular, the difference between new and old models in the location as well as in the temperature width of the instability strip is on average smaller than 200 K. However, the spatial resolution somehow affects the pulsation properties. The new fine models predict a period at the center of the Hertzsprung Progression ($P_{HP} = 9.65-9.84$ days) that reasonably agree with empirical data based on light curves ($P_{HP} = 10.0 \pm 0.5$ days; Moskalik, Buchler, and Marom 1992) and on radial velocity curves ($P_{HP} = 9.95 \pm 0.05$ days; Moskalik et al. 2000), and improve previous predictions by Bono, Castellani, and Marconi (2000, hereinafter BCM00).

Subject headings: Cepheids – Galaxy: stellar content – hydrodynamics – stars: evolution – stars: oscillations

1. Introduction

The EOS and the opacity are fundamental physical ingredients for both evolutionary and pulsation models. In particular, hydrodynamical models of variable stars, when compared with static stellar structures, do require additional derivatives of thermodynamic quantities (Christy 1969; Stellingwerf 1974, 1982, and references therein). As a consequence, the EOS, the opacities, and the numerical methods adopted to estimate physical quantities such as pressure, temperature, internal energy, molecular weight, and their derivatives, are crucial to properly compute the physical structure of stellar envelopes (Dorman, Irwin, and Pedersen 1991). Recent helioseismic data uncorked several theoretical investigations aimed at improving the accuracy of input physics currently adopted to construct both solar and stellar models (see e.g. Christensen-Dalsgaard et al. 1996; Degl'Innocenti et al. 1997; Castellani et al. 2002). The EOS is typically provided in tabular form, where thermodynamic quantities are provided for each given chemical composition as a function of temperature and density.

The most popular ones are the so-called Mihalas-Däppen-Hummer (MHD) EOS (Mihalas, Däppen, and Hummer 1988; Däppen et al. 1988; Däppen, Anderson, and Mihalas 1987) and the OPAL EOS developed at Livermore (Rogers 1986; Iglesias and Rogers 1995; Rogers, Swenson, and Iglesias 1996) and recently improved in the treatment of input physics (Rogers 2000, 2001; Rogers and Nayfonov 2002).

To overcome the problems introduced by the interpolation across the tables, new EOSs have also been developed in the form of in-line analytical formulae that allow the estimate of thermodynamic quantities as a function of temperature, density, and chemical composition. The most recent ones are: EFF (Eggleton, Faulkner, and Flannery 1973), CEFF (Christensen-Dalsgaard and Däppen, 1992), Swenson-Irwin-Rogers-Eggleton-Faulkner-Flannery (SIREFF; see, e.g., Guzik and Swenson 1997), and the recent in-line EOS developed by Irwin[1] (Cassisi, Salaris, and Irwin 2003; Irwin et al. 2003). The reader interested in a detailed discussion concerning pros and cons of the different physical assumptions adopted to derive these EOSs is referred to the reviews by Däppen, Keady, and Rogers (1991), Rogers and Iglesias (1998), and by Däppen and Guzik (2000).

Detailed numerical experiments concerning the dependence of pulsation predictions on the EOS were performed by Kanbur (1991, 1992). He found that both linear and nonlinear radiative Bump Cepheid models constructed by adopting either the MHD EOS or the canonical Saha EOS present negligible differences. However, more recent EOS calculations, when compared with previous ones, do include a more detailed treatment of heavy elements and of the most important Hydrogen molecules. As a consequence, we decided to investigate the dependence of current pulsation predictions for classical Cepheids on the input physics, and in particular on the EOS by taking advantage of the analytical EOS developed by Irwin. Moreover, recent theoretical investigations bring forward that the Mass-Luminosity (ML) relation might play a fundamental role to account for actual properties of variable stars (Bono, Castellani, and Marconi 2002; Bono et al. 2002). Therefore, we also plan to test the dependence on this key ingredient as well as on the spatial resolution across the H and the He ionization regions. The theoretical framework adopted for constructing linear radiative and nonlinear, convective models has already been described in a series of papers (Bono and Stellingwerf 1994; Bono, Marconi, and Stellingwerf 1999, hereinafter BMS99; BCM00, and references therein). The treatment of the EOS is described in Stellingwerf (1975, 1982), while the treatment of the opacities is discussed in Bono, Incerpi, and Marconi (1996).

In section 2 we present the method adopted for handling the opacity tables together with the comparison between the old EOS by Stellingwerf and the new one by Irwin. In

[1]See also ftp://astroftp.phys.uvic.ca/pub/irwin/eos

section 3 and 4 we present detailed theoretical investigations aimed at testing the dependence of theoretical observables predicted by hydrodynamical models for Galactic Cepheids on the input physics. To investigate the linear pulsation behavior we constructed a set of nonadiabatic radiative models. The linear observables, namely period and blue boundary of the instability strip, are widely discussed in section 3.1 and 3.2. We also constructed nonlinear and time-dependent convective Cepheid models to assess the modal stability and, in turn, to evaluate both the boundaries of the strip as well as the amplitude and the morphology of light and velocity curves (section 4.1 and 4.2). Theoretical predictions are also compared with observational data available in the literature. Finally, section 4.3 is focused on the Hertzsprung-Progression (HP). A summary of the results is given in section 5 together with a brief discussion concerning future plans.

2. Input physics

2.1. The opacity

The pulsation models are constructed by adopting radiative opacities (OPAL; Rogers and Iglesias 1992, Iglesias and Rogers 1996) for temperatures higher than $\sim$ 6000 K and molecular opacities (Alexander and Ferguson 1994, hereinafter AF) at lower temperatures. The method adopted to handle the opacity tables, and to evaluate the opacity derivatives with respect to temperature and density, is a revised version of the method described by Bono, Incerpi, and Marconi (1996). It relies on bicubic interpolating functions with analytical derivatives whose coefficients are computed from the functions and the derivatives at grid points (Seaton 1993). In the previous approach, for each given chemical composition, two distinct programs were developed to compute a finer opacity table by interpolating the original OPAL and AF tables. Together with the opacity, the opacity derivatives with respect to temperature and density were also calculated and stored. The previous tables were matched together for a temperature equal to 10,000 K. Finally, the opacity and its derivatives were computed by means of a bilinear interpolation on the finer big table.

The revised method only relies on bicubic spline interpolations. The original two sets of opacity tables (OPAL and AF) are first matched together, then the bicubic spline and its derivatives are computed directly inside the pulsation codes, for the entire range of temperature and density covered by the original table. The temperature value we adopted to match the two sets of opacities is $T = 6300$ K (VandenBerg et al. 2000), since in this temperature range the opacity variations are smooth. Moreover, at lower temperatures, the density range has been extended from $\log R = 1.0$ up to $\log R = 7.0$, where $R = \rho/{T_6}^3$, $T_6 = 10^{-6}\ T$, and ρ is the density. The new method allowed us to decrease by approximately a factor of ten

the CPU time required to construct nonlinear models.

To investigate whether the method adopted to interpolate the opacity tables affects the structure of pulsating models, we performed several numerical experiments across the instability strip. Figure 1 shows the relative difference in opacity between the old and the new interpolation method for three Cepheid models at solar chemical composition, namely $Y = 0.28$, and $Z = 0.02$. The adopted stellar mass ranges from 5 $M_{\odot}$ to 13 $M_{\odot}$, while the effective temperature ranges from $T_e = 5600$ K to $T_e = 3800$ K. The difference is on average smaller than 1 % and approaches 2 % at $\log T \approx 3.8 - 4.0$ K, i.e. the region where the radiative (OPAL) and the molecular (AF) opacity tables were matched together (6300 vs 10,000 K). This indicates that the two methods approach the accuracy of opacity tables that is typically of the order of 2 % (Seaton 1993). Note that to avoid spurious wiggles in the comparison between the two interpolation methods due to small changes in the zoning of the models (Guzik and Swenson 1997), we computed at first the models with the old method and then we used the same values of temperature and density of the individual models to interpolate the opacity tables with the new method. The marginal difference between the two interpolation methods is further supported by the fact that two independent sets of linear models constructed by adopting the old and the new interpolation method present a negligible difference both in the pulsation period and in the growth rate (see data listed in the top of Table 1).

2.2. The equation of state

Pulsation models constructed by our group rely on the equation of state developed by Stellingwerf (1975, 1982). It treats equilibrium mixture of H, H^+, He, He^+, He^{++}, M, and M^+, where M designates a fictional *metal* with fixed ionization potential, number abundance, atomic weight, and degeneracy ratio. These parameters were chosen by fitting the electron pressure at cool temperatures given by an exact solution of King IVa ($Y = 0.28$, $Z = 0.02$) chemical composition (Cox, King, and Tabor 1973). This fictional element was included to account for the ionization of Mg, Fe, and Si in cooler Cepheid envelopes (Stellingwerf 1982).

The accuracy in opacity and EOS derivatives is a key feature to construct accurate pulsation models, since the driving mechanisms are connected with envelope regions where the temperature and the density gradients present sudden changes. Therefore, we decided to improve our hydrodynamical codes by adopting the analytical EOS developed by Irwin, since it is based on approximately the same physics adopted in recent EOS such as MHD and OPAL, and it is quite flexible. We adopted the option suggested by Irwin (*EOS1*) that was

constrained by fitting the OPAL and the SCVH (Saumon, Chabrier, and van Horn 1995) EOSs. The high numerical complexity typical of in-line routines was partially overcome, by selecting some input parameters that allow a sound compromise between speed and accuracy. The flexibility is the main advantage in using an analytical EOS, since it can cope with variations in chemical composition and in elemental mixture. Moreover, an analytical EOS provides smooth high-order derivatives of physical quantities and it can also be easily modified to compute additional thermodynamic quantities. On the other hand, the tabular EOS requires a limited amount of CPU time to interpolate the physical quantities when compared with the in-line EOS. Although, the tabular EOS might be limited in the $\log T$ vs $\log \rho$ coverage as well as in chemical compositions, and does not include high-order derivatives of thermodynamic quantities (Guzik and Swenson 1997; Däppen and Guzik 2000). The latter problem is generally overcome by computing numerical derivatives.

Keeping in mind these problems, we decided to investigate the key features of EOSs available in the literature. The Irwin EOS includes neutral and positive ions of the 20 most abundant atoms, namely: H, He, C, N, O, Ne, Na, Mg, Al, Si, P, S, Cl, A, Ca, Ti, Cr, Mn, Fe, Ni. On the other hand, the tabular EOS by MHD and OPAL only include the elements H, He, C, N, O, and Ne, with the last one that is considered as representative of heavier elements (Rogers, Swenson, and Iglesias 1996; Rogers and Nayfonov 2002). The Irwin EOS allows the use of different solar element mixtures, and therefore the possibility to use the same mixture adopted in the calculation of opacity tables. Note that an EOS that accounts for molecular species might play an important role in constructing pulsation models for long-period-variables such as Semi-Regular, Miras and long-period Cepheids. The OPAL project recently provided new EOS tables that include H_2, H_2^+ as well as H^-, He_2^+, and HeH^+ (Rogers and Nayfonov 2002), while the Irwin EOS only includes the hydrogen molecules. However, previous authors[2] found that in physical regimes where the EOS shows rapid changes, and the density is lower than $\log \rho < -8$, typical of Cepheid envelopes at temperatures cooler than 60,000 K, first order properties, such as pressure and internal energy, might be off by as much as a few percents, while second order properties such as specific heat and adiabatic exponents might be off by as much as 10 %.

In this context, it is worth noting that the main difference in dealing with linear and nonlinear pulsation models is that the latter ones require the second derivatives of total pressure (see eq. A21-A23 in Stellingwerf 1982). These quantities are not generally included in tabular EOSs, and to compute them it is necessary to perform numerical derivatives across the tables. This means that the second derivatives are likely less accurate than the other

[2]See also http://www-phys.llnl.gov/Research/OPAL/index.html

thermodynamic quantities. To compromise between accuracy and numerical complexity, we decided to use the Irwin EOS to compute several tabular EOS at fixed chemical composition but with different grid spacings. The resolution in temperature and density of the tabular EOS need to be cautiously treated, since the interpolation across the tables or the estimate of numerical derivatives might be affected by systematic uncertainties if the grid resolution is too coarse (Dorman, Irwin, and Pedersen 1991). We performed several numerical experiments to overcome this problem, and we found that EOS tables with a step ranging from ~ 0.05 dex to ~ 0.1 dex in $\log T$ and 0.5 dex in $\log R$ works quite well. Figure 2 shows the relative difference in four physical quantities between the analytical and the tabular EOS by Irwin for a 9 $M_{\odot}$ model with $T_e = 4800$ K. From top to bottom the figure shows the relative difference in the adiabatic exponent Γ_1 (Cox and Giuli 1968), internal energy E, mean molecular weight per particle μ, and specific heat at constant pressure C_p. Data plotted in this figure suggest that the difference is typically smaller than 1 %, while for C_p it attains the 2 % across the Hydrogen Ionization Region (HIR). Note that, to perform the difference, we constructed at first the linear model using the tabular EOS and then we used the same values of temperature and density to estimate with the analytical EOS the same physical quantities. Current finding is further supported by the fact that the difference in pulsation periods and growth rates between linear Cepheid models constructed by adopting the analytical EOS and the tabular EOS is at most of the order of a few thousandths (0.003, see data listed in the middle of Table 1).

We performed the same test using a wide range of stellar input parameters and the outcome was the same. This means that the current approach allow us to derive thermodynamic quantities and their derivatives with an accuracy that is on average better than 2 %. The method adopted for interpolating tabular EOS and to derive high-order derivatives is the same adopted for the opacity tables (see Section 2.1). Note that current method uses bicubic splines that provide the opportunity to derive analytical first and second order derivatives instead of estimating them numerically. As a matter of fact, we computed with the analytical Irwin EOS the first derivatives of pressure with respect to temperature and density, then the interpolation with the bicubic splines allowed us to derive analytically the three second-derivatives of pressure. At the same time, we computed with the analytical EOS the specific heat at constant pressure and the interpolation provided the analytical first-derivatives with respect to temperature and density.

3. Linear results

3.1. Dependence on the EOS

To investigate the dependence of pulsation properties on the EOS, we constructed a survey of linear, nonadiabatic models at solar chemical composition, namely $Y = 0.28$, $Z = 0.02$. The luminosity of Cepheid envelope models was fixed according to the ML relation recently derived by Bono et al. (2000). This relation relies on several sets of evolutionary models and agrees quite well with similar prescriptions available in the literature. The difference between the current ML relation and the ML relation provided by Alibert et al. (1999) and by Castellani, Chieffi, and Straniero (1992) is, at fixed stellar mass, on average smaller than 0.1 dex. To constrain the effect of the EOS, we selected three Cepheid models that cover a substantial portion of the instability strip. In particular, the model with 5 $M_{\odot}$ is located close to the fundamental blue edge ($T_e = 5600$ K), the 9 $M_{\odot}$ model is approximately located in the middle of the strip ($T_e = 4800$ K), while the 13 $M_{\odot}$ model is close to the red edge ($T_e = 3800$ K).

Current numerical experiments show that the relative difference in Γ_1 and in C_p is generally smaller than the uncertainties due to the interpolation scheme (see Fig. 2). However toward lower temperatures, the difference between the two EOSs increases and becomes of the order of 15 % (Γ_1) and 30 % (C_p) close to the surface of these envelope structures. The relative difference in the mean molecular weight, μ, presents a systematic trend but it is vanishing (smaller than 1 %) throughout the entire envelope. On the other hand, the difference in the internal energy attains vanishing values (smaller than 1 %) over a substantial portion of the envelope, it undergoes a sudden increase in the outermost regions ($T \leq 10,000$ K), and approaches a difference of the order of 50-60 % close to the surface. Note that to avoid spurious wiggles in the comparison between the two EOSs, we constructed at first the models with the analytical Stellingwerf EOS and then we used the same values of temperature and density to interpolate the tabular Irwin EOS.

Even though some physical quantities present a sizable difference between the Stellingwerf and the Irwin EOS, the impact of this difference on linear observables such as pulsation periods and growth rates is negligible. The difference in the linear periods (fundamental, first, and second overtone) is at most a few hundredths (see data listed in the bottom of Table 1). The same outcome applies for the growth rates. The negligible difference between the two sets of models is due to the marginal effect that the outermost layers have on the pulsation properties.

3.2. Blue boundaries

To investigate the dependence of the blue (hot) edges of the Cepheid instability strip on the EOS, we constructed several sequences of models with stellar masses ranging from 5 to 13 $M_{\odot}$. As in previous investigations (BMS99), the adopted effective temperature step is 100 K. Current ML relation predicts, for each given stellar mass, a luminosity level that is on average lower than adopted by BMS99 and by BCM00. The difference in luminosity is vanishing in the low-mass range but increases when moving toward higher stellar masses. The main intrinsic properties of hydrostatic envelopes and the basic assumption on the numerical approximations adopted for constructing the models have already been discussed in a series of previous papers (see, e.g., Bono and Stellingwerf 1994; BMS99; BCM00). The new models, when compared with the old ones, present a finer spatial resolution in the region located between the first Helium Ionization Region (HeIR, $T \approx 2.1 \times 10^4$ K) and the surface. The number of zones in this region is typically 35, i.e. $\Delta T \approx 450 - 520$ K, while in the old ones was ≈ 25, i.e. $\Delta T \approx 600 - 680$ K. The inner boundary condition was fixed in such a way that the base of the envelope is located at a distance $r_0 = r/R_{ph} = 0.03 - 0.04$ from the star center, where R_{ph} is the equilibrium photospheric radius, while in the old models it was fixed at $r_0 = r/R_{ph} \approx 0.1$. The envelope mass ranges from 65 % to 40 % of the total mass when moving from hotter (5 $M_{\odot}$) to cooler (13 $M_{\odot}$) Cepheid models.

To investigate the dependence of the blue edges on the equation of state, we constructed two independent sets of linear models according to the Stellingwerf and the Irwin EOSs. Current numerical experiments show that the location of fundamental (F) and first-overtone (FO) linear blue boundaries mildly depend on the adopted EOS. The F edges based on the Irwin EOS either are identical, in the low-mass regime, to the edges based on the Stellingwerf EOS or they present a difference at most of 200 K for $M/M_{\odot} = 9$. The difference for FO edges is even smaller and at most of ~ 100 K. However, it turns out that the spatial resolution and the ML relation affect the linear blue boundaries more than the EOS. In fact, the new F blue edge is on average 200 K hotter than predicted by BMS99, and the difference becomes ~ 400 K for stellar masses ranging from 7 to 9 $M_{\odot}$. Note that the difference in the predicted luminosity for $M/M_{\odot} = 5$ between Bono et al. (2000) and BMS99 ML relations is vanishing. Therefore, the difference of 300 K between new and old F and FO blue edges is due to the increase in the spatial resolution of the new models.

4. Nonlinear results

4.1. The instability strip

Nonlinear and time-dependent convective hydrodynamical models supply the unique opportunity to estimate both the blue and the red edge of the instability strip as well as to provide robust predictions concerning the pulsation amplitudes, and the shape of light and velocity curves along the pulsation cycle. This means that observables predicted by nonlinear models can be soundly compared with actual properties of variable stars. To supply a new homogeneous scenario, we constructed six new sequences of nonlinear models with stellar masses ranging from 5 to 13 $M_{\odot}$. The nonlinear analysis was performed by perturbing the linear F and FO radial eigenfunctions with a velocity amplitude of 5 Km s^{-1}. Table 2 summarizes the input parameters as well as the nonlinear pulsation properties of the entire set of models. The observables listed in this table have been estimated at full amplitude, i.e. after that the perturbed envelopes approached the nonlinear limit cycle stability (see BMS99 for more details).

To investigate the dependence of nonlinear pulsation models on the EOS we also computed six sequences of pulsation models by adopting the same assumptions and input parameters of the models listed in Table 2, but by adopting the Stellingwerf EOS. The observables predicted by these models are given in Table 3[3]. The top panel of Figure 3 shows the comparison between nonlinear F and FO edges predicted by models that use the Stellingwerf (triangles) or the Irwin (circles) EOSs. Once again data plotted in this panel disclose that the difference is smaller than 100 K. The same outcome applies for the temperature width, and indeed it decreases by 200 K for stellar masses across the so-called Hertzsprung Progression[4] (HP), i.e. $M \approx 6.55, 7\, M_{\odot}$, while for the other mass values the difference is ≤ 100 K. Moreover, data listed in Tables 2 and 3 show that the relative difference in periods between models constructed by adopting the Stellingwerf EOS and the models based on the Irwin tabular EOS is smaller than 1 % across the entire instability strip. These findings, together with the results obtained for the linear blue edges, indicate that the EOS has a marginal effect on the topology of the Cepheid instability strip.

To single out the effect of the ML relation on pulsation properties we also constructed a new sequence of nonlinear models for $M = 11\ M_{\odot}$ and $\log L/L_{\odot} = 4.40$ (see Table 4). These

[3]This Table is only available in the on-line edition of the manuscript.

[4]In the period range from 6 to 16 days classical Cepheids present a well-defined Bump along both the luminosity and the radial velocity curve. For periods shorter than ≈ 9 days the Bump is located along the decreasing branch, while toward longer periods it takes place along the rising branch.

models when compared with the sequence of models for $M = 11\,M_{\odot}$ listed in Table 2, only differ in the luminosity level (4.40 [BCM00] vs 4.21 [Bono et al. 2000]). The comparison between the observables given in Table 2 and 4 shows that the dependence of the instability strip on the ML relation is mild. The shift in temperature of the new edges is typically smaller than 200 K, while the pulsation amplitudes attain quite similar values.

To investigate the dependence of the pulsation behavior on the spatial resolution across the HIR, we constructed a new sequence of nonlinear models for $M = 11\,M_{\odot}$ by adopting the same input parameters of models listed in Table 2, but a coarse zoning (see Table 5). Data listed in Tables 2 and 5 disclose that the spatial resolution affects the modal stability, and indeed the F edges shift by ≈ 200 K toward hotter effective temperatures. This finding is also supported by the set of models for $M = 5\,M_{\odot}$ listed in Table 3. These models and the set of models for $M = 5\ M_{\odot}$ constructed by BCM00 present the same luminosity, but the comparison displays a shift of $200 - 300$ K in the F edges. Moreover, finer models present an increase in the temperature width of the instability region, namely 1000 vs 600 K for the $M = 5\,M_{\odot}$ models and 900 vs 700 K for the $M = 11\,M_{\odot}$ models. At the same time, the region where FO are pulsationally unstable increases (500 vs 300 K), while the difference in the temperature width for F pulsators is marginal (600 vs 500 K). Note that the increase in the spatial resolution also affects the pulsation amplitudes, and indeed the fine zoning models present, at fixed distance from the blue edge, bolometric amplitudes that are 10 % larger than the coarse zoning models. This difference is even greater (~ 25 %) for the $M = 5\,M_{\odot}$ FO models.

The bottom panel of Figure 3 shows the comparison between the new F and FO edges (circles) and the edges predicted by BCM00 (pluses). A glance at the data plotted in this panel shows that the topology of the instability strip predicted by old and new models is quite similar.

Figures 4, 5, 6, 7, 8, and 9 display both light and velocity curves as a function of phase over two consecutive pulsation cycles for the entire set of models[5]. The comparison between these figures and predictions obtained for the set of models listed in Table 3 further strengthens the evidence that the EOS also marginal affects the morphology of light and velocity curves.

[5]The figures 4, 7, 8, and 9, as well as figures 12 and 13 are only available in the on-line edition of the manuscript.

4.2. Pulsational amplitudes

Nonlinear models also predict the luminosity amplitude, that is a key parameter to study the pulsational properties of classical Cepheids. In particular the Bailey Diagram, i.e. luminosity amplitude versus period, is only marginally affected by reddening and distance uncertainties. Therefore, the comparison between theory and observations in this plane supplies independent constraints on the intrinsic Cepheid parameters to be compared with evolutionary prescriptions. The top panel of Figure 6 shows predicted bolometric amplitudes of Cepheid models constructed by adopting the new (solid line) and the old (dotted line) EOS as a function of period. The agreement between the two sets of models is very good over the entire mass range. The first overtone models for $M = 5\,M_{\odot}$ and the fundamental models across the HP present a mild difference on the EOS close to the edges of the instability region. Data plotted in the middle panel show the dependence of bolometric amplitudes on ML relation and spatial resolution when the Stellingwerf EOS is adopted in the computations. As a whole, the bottom panel displays the comparison between new predictions and old results by BCM00. The predicted luminosity amplitudes show a *hook* shape when moving from the blue to the red edge of the instability region, while the models located across the HP present the typical *double-peaked* distribution of Bump Cepheids (Bono, Marconi, and Stellingwerf 2000, hereinafter BMS00). This trend supports the empirical evidence for Galactic Cepheids originally brought forward by Sandage and Tammann (1971) and by Cogan (1980). They found that in the period range from $\log P \approx 0.40$ to 0.86 and for $\log P > 1.1$-1.3 the largest luminosity amplitudes are attained close to the blue edge, while across the HP ($0.85 \leq \log P \leq 1.1$-1.3) the maximum is attained close to the red edge (BCM00, BMS00).

4.3. Hertzsprung Progression

The top panel of Figure 7 shows the comparison between predicted V-band amplitudes and empirical data for Galactic Cepheids collected by Fernie et al. (1995), while the bottom panel displays the comparison between predicted and empirical radial velocities. Theory is in reasonable agreement with observations. The models across the HP deserve a more detailed discussion. According to BMS00 the secondary minimum in the luminosity and in the velocity amplitude of classical Cepheids located at $\log P \approx 1$ can be adopted to fix the period of the HP center (P_{HP}). They found that for LMC Cepheids $P_{HP} = 11.24 \pm 0.46$ days, while current models for Galactic Cepheids suggest that it is located between $P_{HP} \approx 9.65$ days ($M = 6.55\,M_{\odot}$, $T_e = 5100$ K) and $P_{HP} \approx 9.84$ days ($M = 7\,M_{\odot}$, $T_e = 5300$ K). Current estimates are in good agreement with empirical data, and indeed Moskalik, Buchler, and

Marom (1992) found that the minimum in the Fourier parameters of Galactic Cepheid light curves is roughly equal to $P_{HP} = 10.0 \pm 0.5$ days, and in reasonable agreement with Moskalik et al. (2000) who found $P_{HP} = 9.95 \pm 0.05$ days using radial velocity curves of 131 Cepheids. This finding confirms the results obtained by BMS00, i.e. an increase in the metal content causes a shift of the HP center toward shorter periods. In fact, for SMC ($Z \approx 0.004$) and LMC ($Z \approx 0.008$) Bump Cepheids, it is located at 11.0 ± 0.5 and 10.5 ± 0.5 days respectively (Beaulieu 1998). Moreover, predicted luminosity and velocity curves plotted in Figures 4 and 5 also disclose that the bump along the light curves crosses the luminosity maximum at shorter periods when compared with the velocity curves. A similar feature was already found by BMS00 for LMC Cepheids. Light and velocity curves displayed in Figure 12 refer to models constructed by adopting the same input parameters of models in Figure 4 ($M = 6.55\,M_{\odot}$, $\log L/L_{\odot} = 3.46$), but the Stellingwerf EOS. Data plotted in this figure, together with data listed in Table 3, show that the EOS also has a marginal effect on Bump Cepheids, and indeed the changes along the pulsation cycle as well as in the HP between the two sets of models are quite small.

To constrain the effect of the ML relation and of the spatial resolution on the HP we computed a new sequence of models for $M = 6.55\,M_{\odot}$ by adopting the same input physics and parameters of the models by BCM00 (see Table 6 and Figure 13).

Data plotted in Figure 12 and 13 are both based on the Stellingwerf EOS, but differ for the luminosity level ($\log L/L_{\odot} = 3.46$ [Bono et al. 2000] vs 3.48 [BCM00]) and for the spatial resolution, since models in Figure 13 are characterized by a coarse zoning across the ionization regions. Interestingly enough, the comparison between these two figures discloses that models constructed by adopting the same input physics, a quite similar luminosity level, but a different zoning causes a shift of the HP center toward longer periods, and in turn a better agreement with empirical data. A glance at the data displayed in Figure 13 shows that for $M = 6.55\,M_{\odot}$ the HP center is, indeed, located at $P_{HP} \approx 9.16$ days ($T_e \approx 5250$). Note that for $M = 7\,M_{\odot}$ the models constructed by BCM00 do not show the HP (see their Fig. 11j in the on-line edition).

Qualitative arguments concerning the shape of the fundamental light curves indicate that also the new models for $M = 5\,M_{\odot}$ show a well-defined bump across the instability region. To assess on a quantitative basis whether theoretical models account for the HP that has been detected among short-period Galactic Cepheids, it is necessary to implement current models with new ones that cover the low-mass range (Bono et al. 2002).

5. Summary and final remarks

We performed several numerical experiments aimed at testing the dependence of pulsation observables predicted by both linear and nonlinear models on input physics. We found that the physical structure of linear models is marginally affected by the interpolation methods, based on bicubic splines, we are currently using to estimate the opacity and its derivatives. Interestingly enough, we also found that both linear and nonlinear convective models are also marginally affected by the adopted EOS. We constructed several sequences of pulsation models at solar chemical composition ($Y = 0.28$, and $Z = 0.02$) using the analytical EOS developed by Stellingwerf and the recent one developed by Irwin. The comparison suggests that the difference in the pulsation amplitudes as well as in the topology of the instability strip is negligible.

We selected the Irwin EOS, since it is available in analytical form and it allows us to change the chemical composition as well as the abundance of individual elements. To compromise between accuracy and numerical complexity we computed with the analytical EOS several tabular EOS by changing the grid resolution in temperature and density. The comparison between models constructed with analytical and with the tabular EOS suggests that the difference is marginal once the step ranges from 0.05 to 0.1 dex in $\log T$ and it is equal to 0.5 dex in $\log R$. *Note that the use of bicubic spline interpolations both for opacity and EOS tables provides the unique opportunity to avoid the calculation of numerical derivatives. The EOS first and second order derivatives are estimated by means of the analytical EOS or by means of analytical derivatives of the interpolating function. The opacity first order derivatives are evaluated by means of analytical derivatives of the interpolating function.*

According to recent theoretical investigations we performed several tests to single out the dependence of pulsation predictions on the ML relation as well as on the spatial resolution across the H and the He partial ionization regions. We found that nonlinear models are marginally affected by ML relations available in the literature. Note that current ML relations rely on evolutionary prescriptions (CCS; ABHA; Bono et al. 2000) that neglect convective core overshooting, mass loss, and rotation. Both the location and the temperature width of the nonlinear instability strip present differences on average smaller than 200 K; while the pulsation amplitudes attain quite similar values. Otherwise, the increase in the spatial resolution across the partial ionization regions somehow affects the pulsation properties of Cepheids. In fact, the instability strip based on finer models moves by approximately 200-300 K toward cooler effective temperatures when compared with models based on a coarse zoning. Moreover, fine zoning models present bolometric amplitudes that are 25 % larger than the coarse zoning models.

As a whole, the differences between current models with new input physics and param-

eters, and predictions by BCM00 marginally affect the overall trend inside the instability strip, since the slopes of both blue and red edges predicted by the two sets of models are quite similar. This finding is strongly supported by the evidence that the Period-Radius (PR) relation predicted by current models at solar chemical composition is the following:

$$\log R = 1.173\,(\pm\,0.008) + 0.676\,(\pm\,0.006)\log P;$$

while the models constructed by BCM00 supply

$$\log R = 1.191\,(\pm\,0.006) + 0.654\,(\pm\,0.005)\log P,$$

where the radius R is in solar units and the period P in days. The difference between these two relations is quite small and ranges from 0.005 to 0.002 dex when moving from $\log P = 0.5$ to $\log P = 1.0$.

Moreover and even more importantly, we found that spatial resolution also affects P_{HP}, i.e. the pulsation period at the center of the Hertzsprung Progression. The new models show that P_{HP} ranges from 9.65 for $M = 6.55\,M_{\odot}$ to 9.84 days for $M = 7\,M_{\odot}$. These estimates, when compared with models constructed by BCM00, agree reasonable well with empirical estimates based on light curves ($P_{HP} = 10.0 \pm 0.5$ days, Moskalik, Buchler, and Marom 1992) as well as on radial velocity curves ($P_{HP} = 9.95 \pm 0.05$ days, Moskalik et al. 2000). Preliminary qualitative results indicate that the new models might also account for the HP that has been detected in the short-period range (Kienzle et al. 1999, and references therein). Current models do account for the shift of P_{HP} toward shorter periods when moving toward more metal-rich stellar systems (BCM00, BMS00). However, more detailed calculations are required to figure out whether current nonlinear pulsation models do account for the *double-peaked* distribution disclosed by Galactic and Magellanic Bump Cepheids in the amplitude vs period plane.

To further constrain the zoning effect, we computed several linear and nonlinear models across the instability strip by increasing the spatial resolution from 35 to ≈ 50, i.e. $\Delta T \approx$ 400 K. We found that the difference between these two sets of models is negligible, and indeed the difference among linear periods and growth rates is smaller than 0.5-1 % across the instability strip. The relative difference among nonlinear observables is even smaller, in particular the shift in temperature of the instability strip is smaller than 100 K, while the change in luminosity and velocity amplitudes is smaller than ~ 0.1 %.

The extension of current theoretical framework to Magellanic Cepheids seems quite promising not only for the intrinsic properties of variable stars but also to figure out whether

the input physics, and/or the spatial resolution of pulsation models do affect the topology of the instability strip, and in turn predictions concerning the PL and the PLC relations. At the same time, we are also interested in performing a more quantitative comparison between predicted and empirical light curves using both the Fourier technique (Ngeow et al. 2003) and the principal component analysis (Kanbur et al. 2002). The main goal of this project is to constrain the accuracy of current pulsation models, and in turn to figure out whether the decomposition parameters can be safely adopted to estimate intrinsic parameters of classical Cepheids.

It is a pleasure to thank A. W. Irwin for detailed information and enlightening suggestions concerning the use of the analytical EOS he developed. We are also grateful to V. Castellani for several enlightening discussions and for a critical reading of an early draft of this manuscript. We wish to warmly thank an anonymous referee for several comments and suggestions that improved the content and the readability of the paper. This work was supported by MIUR/COFIN 2002 under the project (#028935): "Stellar Populations in Local Group Galaxies".

REFERENCES

Alexander, D. R., and Ferguson, J. W. 1994, ApJ, 437, 879

Alibert, Y., Baraffe, I., Hauschildt, P., and Allard, F. 1999, A&A, 344, 551

Beaulieu, J. P. 1998, MmSAI, 69, 21

Bersier, D. and Burki, G. 1996, A&A, 306, 417

Bono, G., Caputo, F., Cassisi, S., Marconi, M., Piersanti, L., and Tornambè, A. 2000, ApJ, 543, 955

Bono, G., Castellani, V., and Marconi, M. 2000, ApJ, 529, 293; BCM00

Bono, G., Castellani, V.,and Marconi, M. 2002, ApJ, 565, 83

Bono, G., Groenewegen, M. A. T., Marconi, M., and Caputo, F. 2002, ApJ, 574, L33

Bono, G., Incerpi, R. and Marconi, M. 1996, ApJ, 467, 97

Bono, G., Marconi, M., and Stellingwerf, R. F. 1999, ApJS, 122, 167; BMS99

Bono, G., Marconi, M., and Stellingwerf, R. F. 2000, A&A, 360, 245; BMS00

Bono, G. and Stellingwerf, R. F. 1994, ApJS, 93, 233

Cassisi, S. Salaris M., and Irwin, A. W. 2003, ApJ, 588, 862

Castellani, V., Chieffi, A., and Straniero, O. 1992, ApJS, 78, 517

Castellani, V., Degl'Innocenti, S., Prada Moroni, P. G., and Tordiglione, V. 2002, MNRAS, 334, 193

Christensen-Dalsgaard, J. and Däppen, W. 1992, A&A Rev., 4, 267

Christensen-Dalsgaard, J. et al. 1996, Sci, 272, 1286

Christy, R. F. 1969, JRASC, 63, 299

Cogan, B. C. 1980, ApJ, 239, 941

Cox, J. and Giuli, R. 1968, Principles of Stellar Structure, (New York: Gordon and Breach), 211

Cox, A. N., King, D. S., and Tabor, J. E. 1973, ApJ, 184, 201

Däppen, W., Anderson, L. S., and Mihalas, D. 1987, ApJ, 319, 195

Däppen, W. and Guzik, J. A. 2000, Variable Stars as Essential Astrophysical Tools, ed. C. Ibanoglu, (Dordrecht: Kluwer Acad. Publ.), NATO Science Series C, 544, 177

Däppen, W., Keady, J., and Rogers, F. 1991, in Solar Interior and Atmosphere, (Tucson: Univ. of Arizona Press), 112

Däppen, W., Mihalas, D., Hummer, D. G., and Mihalas, B. W. 1988, ApJ, 332, 261

Degl'Innocenti, S., Dziembowski, W. A, Fiorentini, G., and Ricci, B. 1997, Astrop. Phys. 7, 77

Dorman, B., Irwin, A. W., and Pedersen, B. B. 1991, ApJ, 381, 228

Eggleton, P. P., Faulkner, J., and Flannery, B. P. 1973, A&A, 23, 325

Fernie, J. D., Evans, N. R., Beattie, B., and Seager, S. 1995, Inf. Bull. Variable Stars, 4148, 1

Guzik, J. A. and Swenson, F. J. 1997, ApJ, 491, 967

Kanbur, S. M. 1991, A&A, 250, 395

Kanbur, S. M. 1992, A&A, 259, 175

Kanbur, S. M., Iono, D., Tanvir, N. R., Hendry, M. A. 2002 MNRAS, 329, 126

Kienzle, F., Moskalik, P., Bersier, D., and Pont, F. 1999, A&A, 341, 818

Iglesias, C. A. and Rogers, F. J. 1995, ApJ, 443, 460

Iglesias, C. A. and Rogers, F. J. 1996, ApJ, 464, 943

Irwin, A. W., Swenson, F. J., VandenBerg, D. A., and Rogers, F. J. 2003, in preparation

Mihalas, D., Däppen, W., and Hummer, D. G. 1988, ApJ, 331, 815

Moskalik, P., Buchler, J. R., and Marom, A. 1992 ApJ, 385, 685

Moskalik, P., Krzyt, T., Gorynya, N. A., and Samus, N. N. 2000, in IAU Colloq. 176, The Impact of Large-Scale Surveys on Pulsating Star Research, ed. L. Szabados and D.W. Kurtz, (San Francisco: ASP), 233

Ngeow, C., Kanbur, S. M., Nikolaev, S., Tanvir, N. R., Hendry, M. A. 2003, ApJ, 586, 959

Rogers, F. J. 1986, ApJ, 310, 723

Rogers, F. J. 2000 Physics of Plasmas, V7(N1), 51

Rogers, F. J. 2001 Contributions to Plasma Physics, V41(N2-3), 179

Rogers, F. J. and Iglesias, C. A. 1992, ApJS, 79, 507

Rogers, F. J. and Iglesias, C. A. 1998, in A Half Century of Stellar Pulsation Interpretation: A Tribute to A. N. Cox, ed. P.A. Bradley and J.A. Guzik, (San Francisco: ASP), 254

Rogers, F. J. and Nayfonov, A. 2002 ApJ, 576, 1064

Rogers, F. J., Swenson, F. J., and Iglesias, C. A. 1996, ApJ, 456, 902

Sandage, A., Tammann, G. A. 1971, ApJ, 167, 293

Saumon, D., Chabrier, G., and van Horn, H. M. 1995, ApJS, 99, 713

Seaton, M. J. 1993, MNRAS, 265, 25

Stellingwerf, R. F. 1974 ApJ, 192, 139

Stellingwerf, R. F. 1975 ApJ, 195, 441

Stellingwerf, R. F. 1982, ApJ, 262, 330

VandenBerg, D. A., Swenson, F. J., Rogers, F. J., Iglesias, C. A., and Alexander, D. R. 2000, ApJ, 532, 430

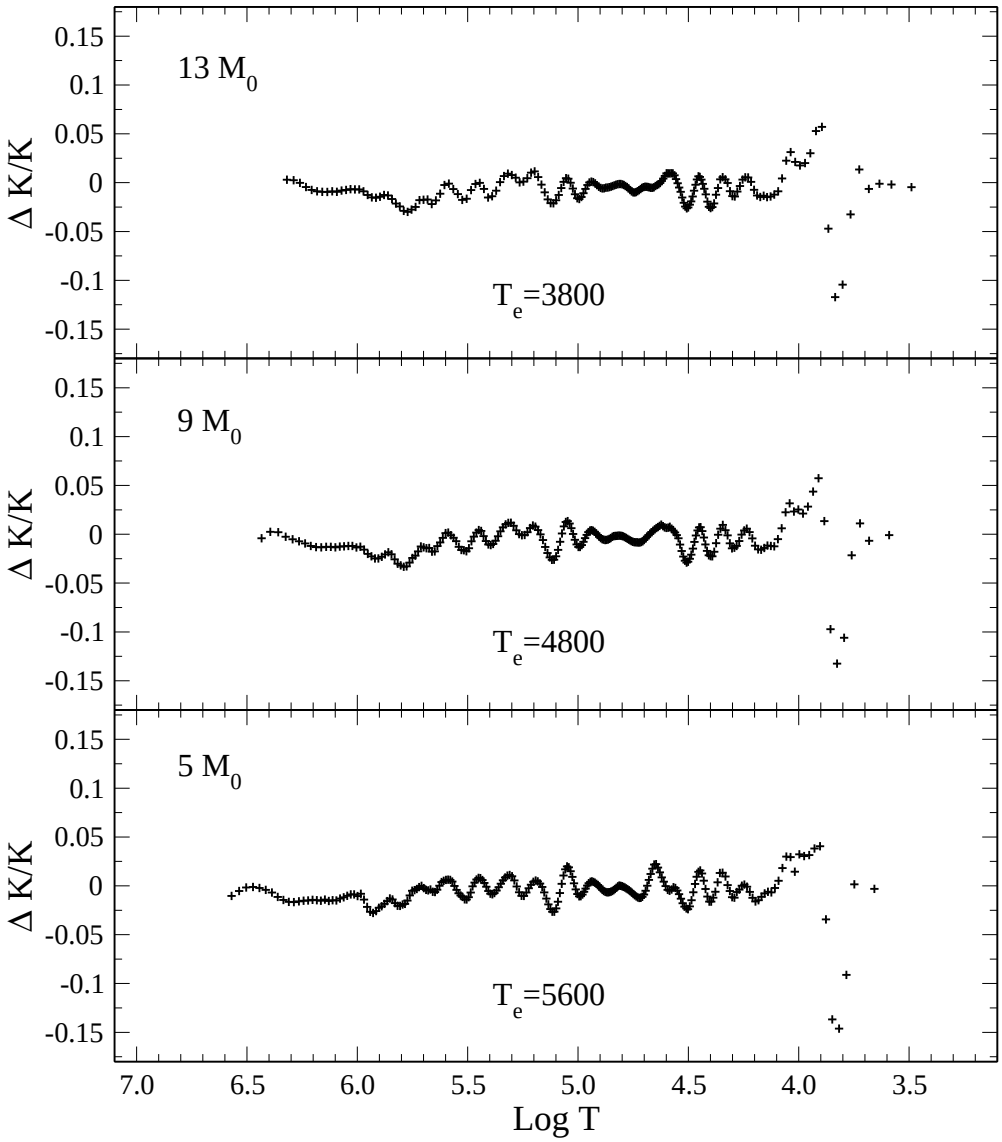

Fig. 1.— Relative difference in opacity between the old and the new method adopted to interpolate opacity tables as a function of logarithmic temperature. From top to bottom data refer to different linear models. See text for more details.

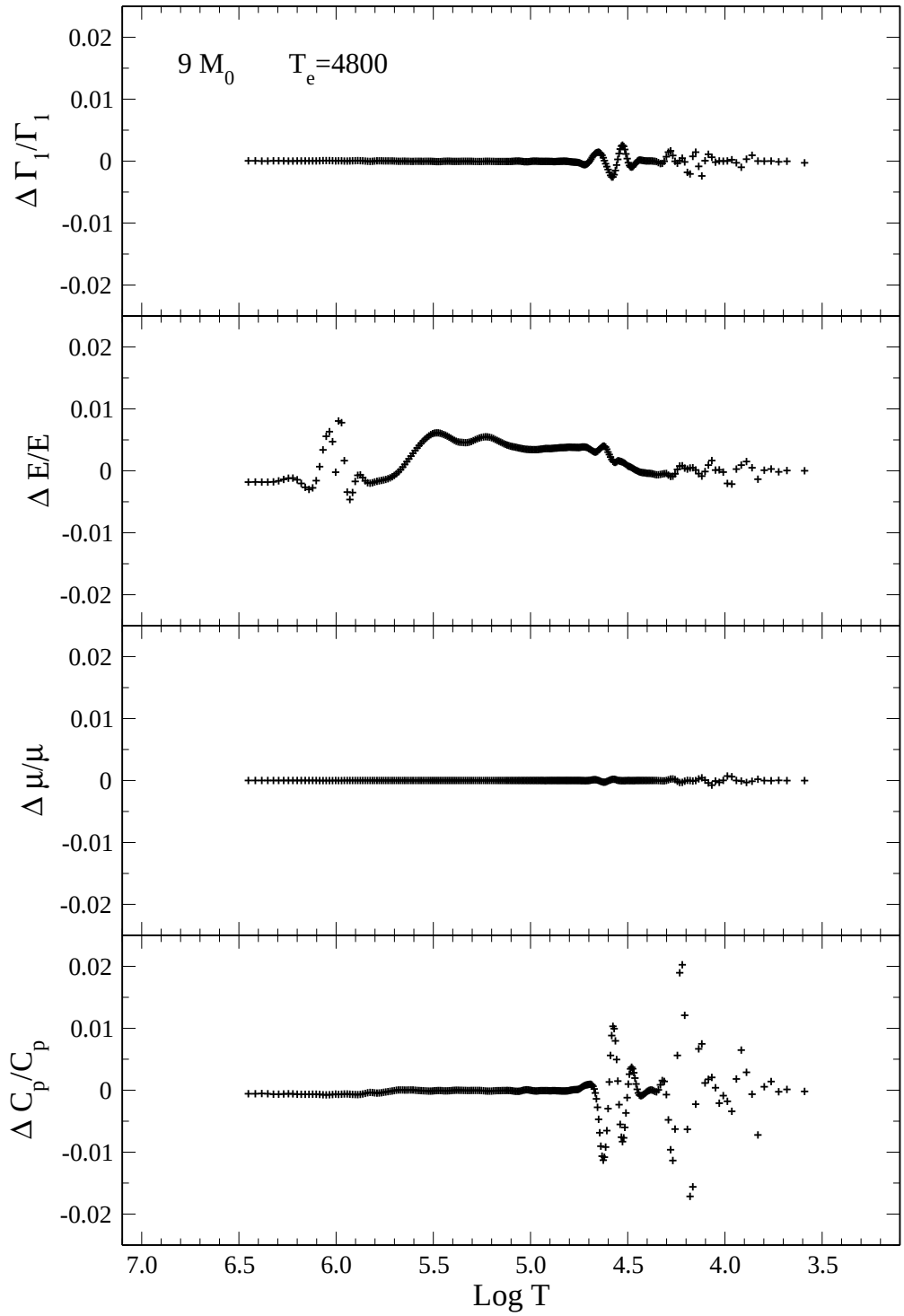

Fig. 2.— From top to bottom relative difference in adiabatic exponent, internal energy, molecular weight, and specific heat at constant pressure between the analytical and the tabular form of the Irwin EOS.

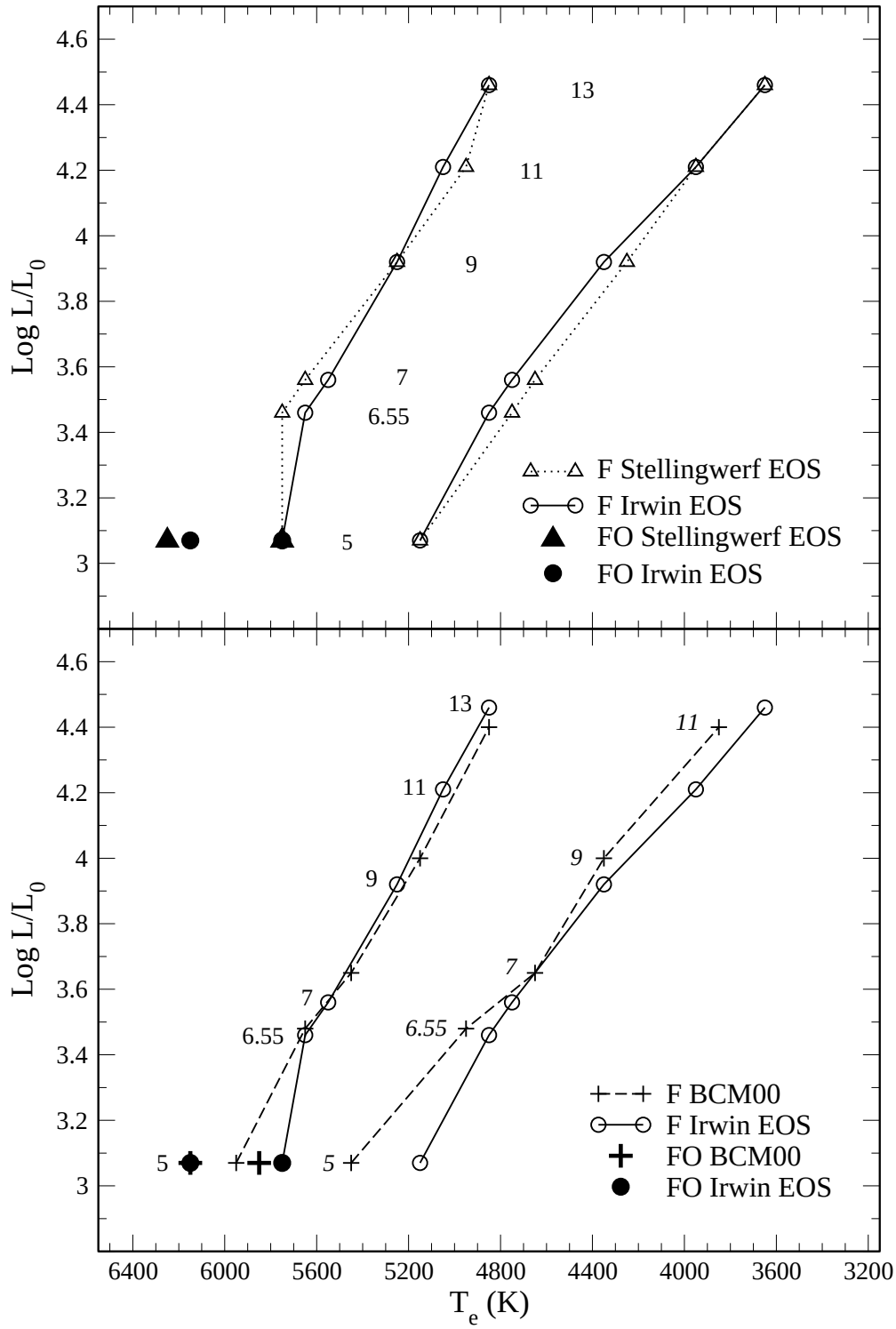

Fig. 3.— Comparison in the HR diagram between nonlinear Fundamental (F) and First Overtone (FO) blue and red edges according to models constructed using different EOS (top panel) or different EOS, ML relation, and spatial resolution (bottom panel). Stellar masses are in solar units.

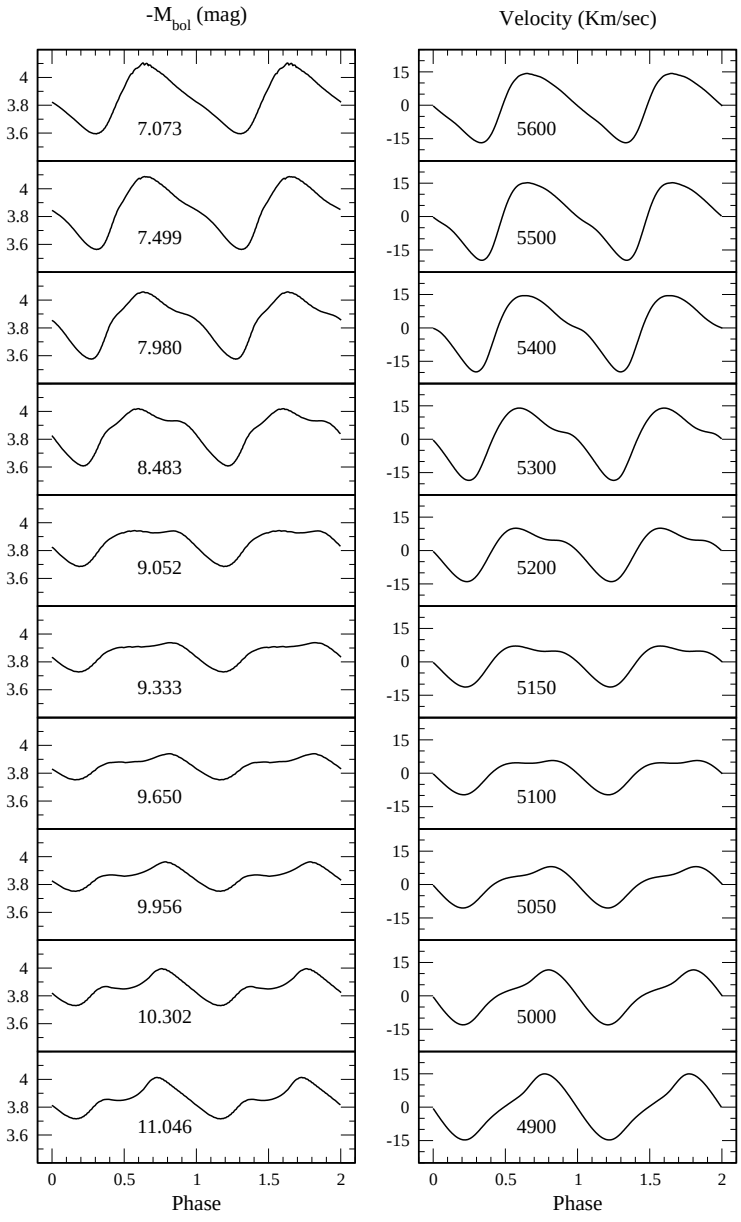

Fig. 4.— Same as Fig. 4, but for the sequence of models with $M = 6.55\,M_{\odot}$.

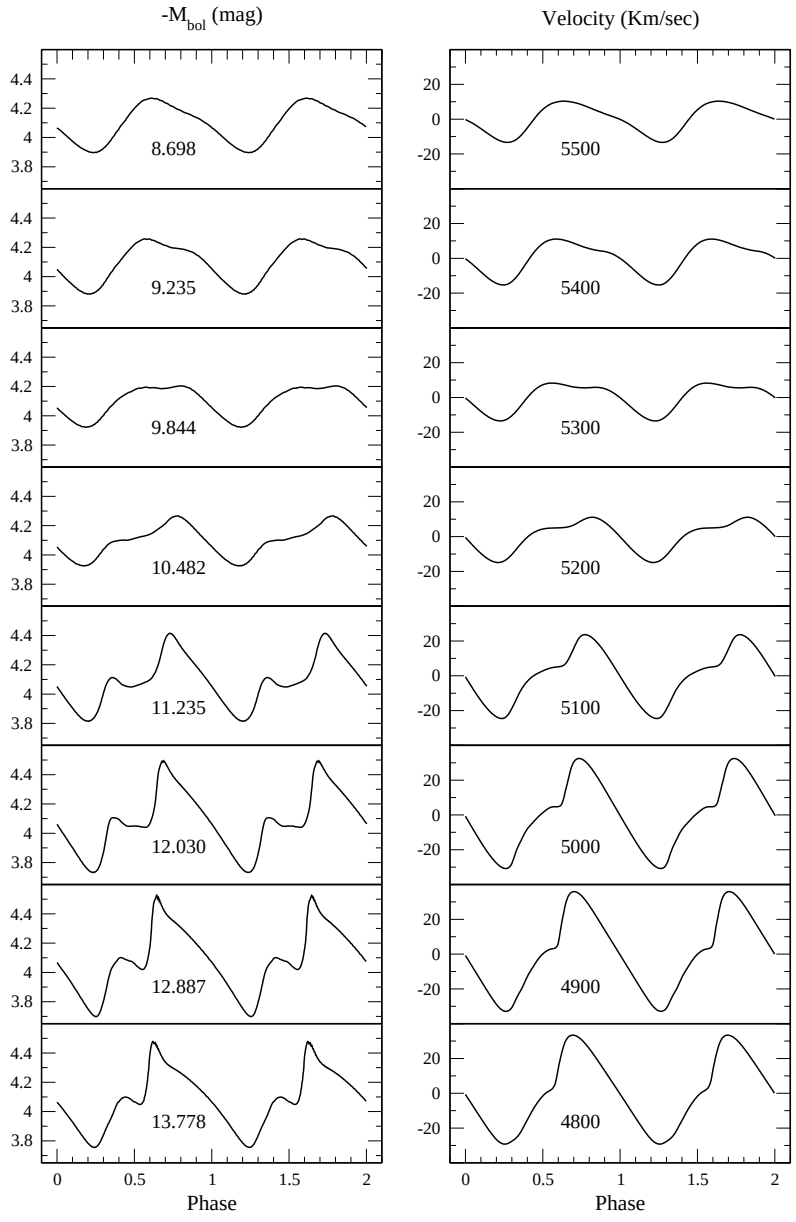

Fig. 5.— Same as Fig. 4, but for the sequence of models with $M = 7\,M_{\odot}$.

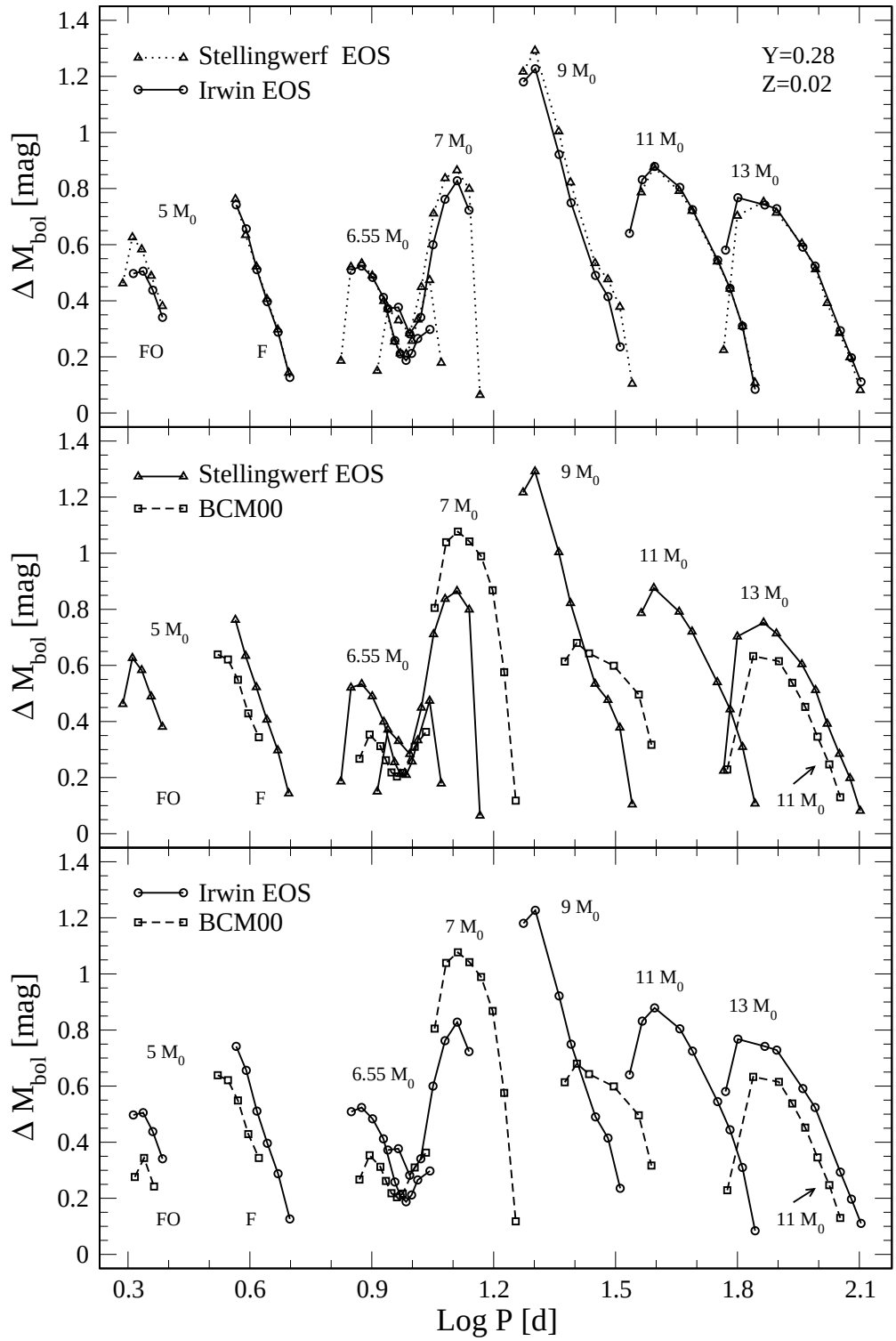

Fig. 6.— Comparison between bolometric amplitudes based on pulsation models constructed by adopting different EOS (top panel), different ML relation, and spatial resolution (middle panel), different EOS, ML relation, and spatial resolution (bottom panel).

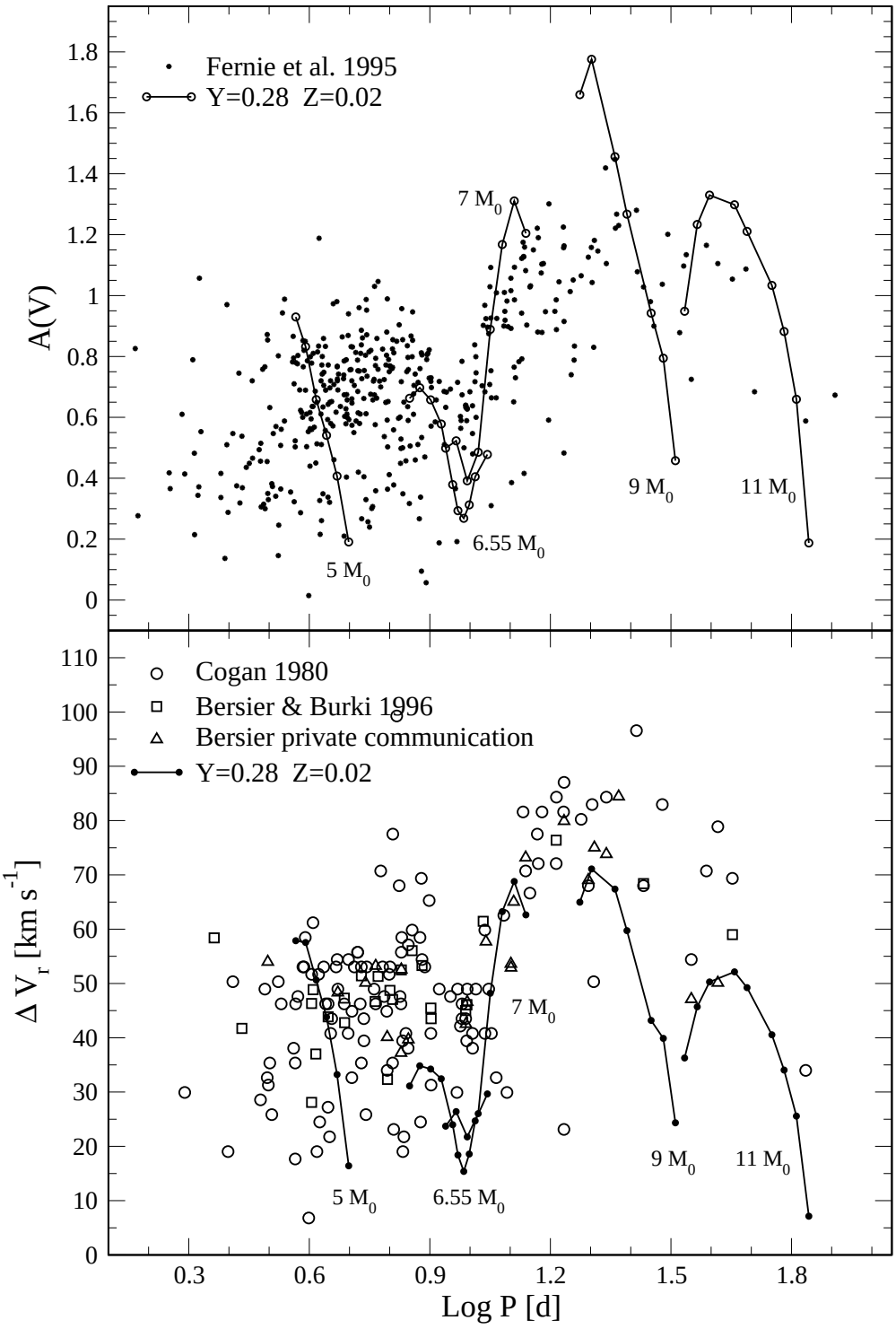

Fig. 7.— Comparison between predicted and empirical amplitudes for fundamental Galactic Cepheids. The top panel shows the comparison between V-band amplitudes collected by Fernie et al. (1995) and current models. The bottom panel displays the comparison between different samples of empirical radial velocity amplitudes and theoretical predictions. Note that predicted amplitudes were multiplied by 1.36 (Bersier and Burki 1996).

Table 1. Relative difference in pulsation periods and growth rates for linear models constructed by adopting different input physics.

			Period			Growth Rate		
M[a]	$logL$[b]	T_e[c]	$\Delta P_0/P_0$[d]	$\Delta P_1/P_1$	$\Delta P_2/P_2$	$\Delta\eta_0/\eta_0$[e]	$\Delta\eta_1/\eta_1$	$\Delta\eta_2/\eta_2$
				Test on Opacity[(1)]				
5.0	3.07	5600	0.0003	0.0004	0.0001	-0.004	-0.014	-0.090
9.0	3.92	4800	0.0003	0.0004	-0.0001	0.005	0.006	0.007
13.0	4.46	3800	-0.0001	-0.0001	-0.0001	-0.003	-0.200	-0.003
				Test on EOS[(2)]				
5.0	3.07	5600	-0.0009	-0.0005	-0.0003	0.003	0.003	0.0005
9.0	3.92	4800	0.003	0.002	0.001	-0.006	0.003	-0.010
13.0	4.46	3800	0.0002	-0.0005	-0.0007	-0.001	0.010	-0.017
				Test on EOS[(3)]				
5.0	3.07	5600	0.004	0.006	0.005	0.05	0.02	-0.02
9.0	3.92	4800	-0.012	-0.030	-0.030	-0.05	-0.02	-0.03
13.0	4.46	3800	-0.003	-0.002	-0.003	-0.03	-0.02	0.01

[a]Stellar mass (solar units).

[b]Logarithmic luminosity (solar units).

[c]Static effective temperature (K).

[d]Relative difference in periods. P_i with $i = 0, 1, 2$ indicates fundamental, first-overtone, and second-overtone periods, respectively.

[e]Relative difference in growth rates. η_i with $i = 0, 1, 2$ indicates the fundamental, first-overtone, and second-overtone growth rates, respectively.

[(1)]The linear models were constructed by adopting two different methods to interpolate the opacity tables (see § 2.1).

[(2)]The linear models were constructed by adopting the analytical Irwin EOS and the tabular form of the same EOS (see § 2.2).

[(3)]The linear models were constructed by adopting the analytical Stellingwerf EOS and the tabular Irwin EOS (see § 3.1).

Table 2. Input parameters and nonlinear observables for first-overtone and fundamental Cepheid models at solar chemical composition.

M[a] (1)	$logL$[b] (2)	T_e[c] (3)	P[d] (4)	$\log \overline{R}$[e] (5)	$\Delta R/R_{ph}$[f] (6)	Δu[g] (7)	ΔM_{bol}[h] (8)	$\Delta \log g_s$[i] (9)	ΔT_e[j] (10)
				First-overtone					
5.0	3.07	6100	2.0565	1.488	0.045	34.87	0.497	0.04	740
5.0	3.07	6000	2.1733	1.502	0.051	39.27	0.505	0.04	728
5.0	3.07	5900	2.2958	1.516	0.050	37.94	0.438	0.04	620
5.0	3.07	5800	2.4253	1.531	0.044	32.38	0.341	0.04	479
				Fundamental					
5.0	3.07	5700	3.6840	1.548	0.115	57.88	0.742	0.10	1037
5.0	3.07	5600	3.8991	1.564	0.120	57.55	0.656	0.11	906
5.0	3.07	5500	4.1422	1.578	0.105	50.63	0.511	0.09	712
5.0	3.07	5400	4.3949	1.593	0.094	43.80	0.396	0.08	610
5.0	3.07	5300	4.6688	1.606	0.074	33.22	0.288	0.07	445
5.0	3.07	5200	4.9913	1.622	0.038	16.42	0.127	0.03	212
6.55	3.46	5600	7.0730	1.758	0.072	31.13	0.509	0.06	703
6.55	3.46	5500	7.4988	1.773	0.079	34.83	0.524	0.07	712
6.55	3.46	5400	7.9803	1.790	0.077	34.24	0.483	0.07	643
6.55	3.46	5300	8.4829	1.804	0.074	32.45	0.412	0.06	554
6.55	3.46	5200	9.0525	1.820	0.059	23.98	0.258	0.05	375
6.55	3.46	5150	9.3328	1.828	0.048	18.40	0.211	0.04	287
6.55	3.46	5100	9.6496	1.836	0.042	15.39	0.188	0.04	223
6.55	3.46	5050	9.9560	1.845	0.047	18.58	0.212	0.04	269
6.55	3.46	5000	10.3025	1.853	0.060	24.68	0.266	0.05	354
6.55	3.46	4900	11.0464	1.869	0.076	29.66	0.298	0.07	418
7.0	3.56	5500	8.6976	1.821	0.057	23.71	0.372	0.05	521
7.0	3.56	5400	9.2348	1.838	0.064	26.40	0.377	0.06	532
7.0	3.56	5300	9.8443	1.853	0.057	21.74	0.282	0.05	394
7.0	3.56	5200	10.4821	1.869	0.064	26.03	0.341	0.06	434
7.0	3.56	5100	11.2346	1.888	0.110	48.21	0.600	0.10	798
7.0	3.56	5000	12.0295	1.908	0.149	63.24	0.762	0.13	1029
7.0	3.56	4900	12.8869	1.926	0.171	68.79	0.828	0.15	1128
7.0	3.56	4800	13.7777	1.941	0.170	62.63	0.723	0.15	1038

Table 2—Continued

M^{a} (1)	$logL^{b}$ (2)	$T_e{}^{c}$ (3)	P^{d} (4)	$\log \overline{R}^{e}$ (5)	$\Delta R/R_{ph}{}^{f}$ (6)	Δu^{g} (7)	$\Delta M_{bol}{}^{h}$ (8)	$\Delta \log g_s{}^{i}$ (9)	$\Delta T_e{}^{j}$ (10)
9.0	3.92	5200	18.7620	1.951	0.198	64.96	1.180	0.17	1721
9.0	3.92	5100	20.0704	2.079	0.220	71.09	1.227	0.19	1751
9.0	3.92	4900	22.9589	2.117	0.218	67.38	0.922	0.19	1283
9.0	3.92	4800	24.5763	2.129	0.204	59.74	0.750	0.18	1116
9.0	3.92	4600	28.2280	2.158	0.174	43.20	0.490	0.15	800
9.0	3.92	4500	30.2840	2.175	0.165	39.88	0.415	0.15	667
9.0	3.92	4400	32.4571	2.188	0.110	24.33	0.236	0.10	363
11.0	4.21	5000	34.2116	2.236	0.232	36.29	0.641	0.21	901
11.0	4.21	4900	36.7837	2.259	0.288	45.70	0.832	0.27	1128
11.0	4.21	4800	39.4572	2.276	0.329	50.28	0.879	0.31	1128
11.0	4.21	4600	45.5276	2.311	0.387	52.14	0.804	0.38	918
11.0	4.21	4500	48.9255	2.326	0.408	49.24	0.725	0.41	845
11.0	4.21	4300	56.4072	2.357	0.436	40.54	0.545	0.46	682
11.0	4.21	4200	60.4930	2.371	0.441	34.06	0.444	0.49	564
11.0	4.21	4100	64.9105	2.385	0.438	25.57	0.310	0.50	416
11.0	4.21	4000	69.7311	2.395	0.405	7.14	0.084	0.49	106
13.0	4.46	4800	58.9766	2.393	0.480	31.59	0.581	0.52	775
13.0	4.46	4700	63.2735	2.412	0.521	39.56	0.767	0.57	942
13.0	4.46	4500	73.6824	2.447	0.565	43.08	0.742	0.65	806
13.0	4.46	4400	78.8145	2.464	0.577	43.43	0.729	0.68	746
13.0	4.46	4200	91.4053	2.496	0.588	35.29	0.591	0.73	597
13.0	4.46	4100	97.9617	2.509	0.587	30.92	0.524	0.76	539
13.0	4.46	3900	113.0619	2.537	0.572	18.45	0.293	0.80	326
13.0	4.46	3800	120.3557	2.549	0.556	12.03	0.197	0.81	220
13.0	4.46	3700	127.1189	2.559	0.535	6.66	0.111	0.82	109

[a]Stellar mass (solar units).
[b]Logarithmic luminosity (solar units).
[c]Effective temperature (K).
[d]Period (day).
[e]Logarithmic mean radius (solar units).
[f]Fractional radius variation.
[g]Radial velocity amplitude (Km s^{-1}).
[h]Bolometric amplitude (mag).
[i]Amplitude of logarithmic static gravity.
[j]Effective temperature variation (K).

Table 3. Same as Table 2, but the models were constructed by adopting the Stellingwerf EOS, the ML relation by Bono et al. (2000), and a fine zoning across Hydrogen and Helium ionization regions.

M[a] (1)	$logL$[b] (2)	T_e[c] (3)	P[d] (4)	$\log \overline{R}$[e] (5)	$\Delta R/R_{ph}$[f] (6)	Δu[g] (7)	ΔM_{bol}[h] (8)	$\Delta \log g_s$[i] (9)	ΔT_e[j] (10)
				First-overtone					
5.0	3.07	6200	1.9373	1.472	0.038	30.12	0.462	0.03	706
5.0	3.07	6100	2.0451	1.488	0.056	44.00	0.626	0.05	932
5.0	3.07	6000	2.1559	1.502	0.057	45.38	0.583	0.05	843
5.0	3.07	5900	2.2745	1.517	0.054	42.07	0.489	0.05	682
5.0	3.07	5800	2.4248	1.531	0.048	36.05	0.381	0.04	526
				Fundamental					
5.0	3.07	5700	3.6675	1.548	0.116	59.33	0.762	0.10	1068
5.0	3.07	5600	3.8855	1.563	0.113	55.74	0.634	0.10	862
5.0	3.07	5500	4.1284	1.578	0.105	50.78	0.522	0.09	724
5.0	3.07	5400	4.3816	1.592	0.094	43.88	0.406	0.08	617
5.0	3.07	5300	4.6624	1.606	0.074	33.33	0.297	0.07	459
5.0	3.07	5200	4.9612	1.622	0.042	17.99	0.143	0.04	238
6.55	3.46	5700	6.6665	1.742	0.026	10.98	0.186	0.02	269
6.55	3.46	5600	7.0588	1.757	0.073	32.08	0.521	0.06	720
6.55	3.46	5500	7.5039	1.774	0.079	35.07	0.533	0.07	725
6.55	3.46	5400	7.9632	1.790	0.077	34.43	0.490	0.07	657
6.55	3.46	5300	8.5037	1.804	0.073	31.50	0.399	0.06	548
6.55	3.46	5200	9.0372	1.819	0.056	22.64	0.255	0.05	365
6.55	3.46	5150	9.3354	1.828	0.046	17.18	0.213	0.04	275
6.55	3.46	5100	9.6520	1.836	0.045	17.22	0.210	0.04	259
6.55	3.46	5050	9.9832	1.845	0.054	22.29	0.257	0.05	334
6.55	3.46	5000	10.3117	1.854	0.071	29.84	0.333	0.06	446
6.55	3.46	4900	11.0254	1.871	0.106	43.62	0.474	0.09	657
6.55	3.46	4800	11.7725	1.886	0.056	19.61	0.179	0.05	271
7.0	3.56	5600	8.1908	1.804	0.022	9.01	0.150	0.02	217
7.0	3.56	5500	8.7064	1.822	0.057	23.74	0.371	0.05	528
7.0	3.56	5400	9.2405	1.837	0.058	23.42	0.330	0.05	475
7.0	3.56	5300	9.8539	1.853	0.054	19.83	0.284	0.05	349
7.0	3.56	5200	10.5189	1.869	0.079	33.87	0.449	0.07	586

Table 3—Continued

M[a] (1)	$logL$[b] (2)	T_e[c] (3)	P[d] (4)	$\log \overline{R}$[e] (5)	$\Delta R/R_{ph}$[f] (6)	Δu[g] (7)	ΔM_{bol}[h] (8)	$\Delta \log g_s$[i] (9)	ΔT_e[j] (10)
7.0	3.56	5100	11.2733	1.888	0.125	55.06	0.711	0.11	942
7.0	3.56	5000	12.0393	1.908	0.157	66.96	0.837	0.14	1118
7.0	3.56	4900	12.8744	1.927	0.174	69.36	0.865	0.15	1181
7.0	3.56	4800	13.8014	1.943	0.180	65.97	0.799	0.16	1135
7.0	3.56	4700	14.6685	1.951	0.023	7.17	0.064	0.02	100
9.0	3.92	5200	18.7266	2.062	0.200	66.06	1.217	0.17	1778
9.0	3.92	5100	20.0248	2.080	0.222	72.40	1.292	0.19	1854
9.0	3.92	4900	22.9230	2.113	0.222	69.25	1.004	0.20	1382
9.0	3.92	4800	24.4934	2.130	0.212	62.75	0.822	0.19	1150
9.0	3.92	4600	28.1603	2.159	0.183	46.07	0.534	0.16	846
9.0	3.92	4500	30.2792	2.177	0.180	43.81	0.476	0.16	740
9.0	3.92	4400	32.4045	2.190	0.154	36.54	0.378	0.14	573
9.0	3.92	4300	34.7587	2.202	0.115	10.86	0.104	0.11	153
11.0	4.21	4900	36.5833	2.257	0.282	43.12	0.787	0.26	1072
11.0	4.21	4800	39.2919	2.274	0.325	48.35	0.876	0.31	1125
11.0	4.21	4600	45.3609	2.311	0.385	50.60	0.791	0.38	909
11.0	4.21	4500	48.7902	2.326	0.407	48.44	0.721	0.41	826
11.0	4.21	4300	56.2860	2.357	0.438	40.30	0.540	0.47	677
11.0	4.21	4200	60.5200	2.372	0.444	34.31	0.443	0.49	565
11.0	4.21	4100	64.9298	2.386	0.441	25.92	0.309	0.51	415
11.0	4.21	4000	69.7022	2.397	0.415	10.08	0.108	0.50	150
13.0	4.46	4800	58.3580	2.389	0.437	13.56	0.224	0.49	314
13.0	4.46	4700	63.0748	2.411	0.516	37.00	0.703	0.57	881
13.0	4.46	4500	73.1909	2.449	0.564	42.79	0.752	0.65	817
13.0	4.46	4400	78.6635	2.465	0.578	42.26	0.714	0.68	734
13.0	4.46	4200	90.9012	2.496	0.591	36.73	0.604	0.74	586
13.0	4.46	4100	98.2004	2.512	0.590	30.99	0.512	0.76	518
13.0	4.46	4000	104.9605	2.525	0.584	24.93	0.392	0.78	420
13.0	4.46	3900	112.4829	2.537	0.574	18.75	0.285	0.80	316
13.0	4.46	3800	119.3546	2.548	0.557	13.01	0.198	0.81	223

Table 3—Continued

M[a] (1)	$logL$[b] (2)	T_e[c] (3)	P[d] (4)	$\log \overline{R}$[e] (5)	$\Delta R/R_{ph}$[f] (6)	Δu[g] (7)	ΔM_{bol}[h] (8)	$\Delta \log g_s$[i] (9)	ΔT_e[j] (10)
13.0	4.46	3700	126.5626	2.558	0.533	5.66	0.081	0.82	92

[a]Stellar mass (solar units).
[b]Logarithmic luminosity (solar units).
[c]Effective temperature (K).
[d]Period (day).
[e]Logarithmic mean radius (solar units).
[f]Fractional radius variation.
[g]Radial velocity amplitude (Km s^{-1}).
[h]Bolometric amplitude (mag).
[i]Amplitude of logarithmic static gravity.
[j]Effective temperature variation (K).

Table 4. Input parameters and nonlinear observables for Cepheid models with $M = 11\,M_{\odot}$ and solar chemical composition. These models were constructed by adopting the Irwin EOS, the ML relation used by BCM00, and a fine zoning across Hydrogen and Helium ionization regions.

M[a] (1)	$logL$[b] (2)	T_e[c] (3)	P[d] (4)	$\log \overline{R}$[e] (5)	$\Delta R/R_{ph}$[f] (6)	Δu[g] (7)	ΔM_{bol}[h] (8)	$\Delta \log g_s$[i] (9)	ΔT_e[j] (10)
11.0	4.40	4800	59.3229	2.364	0.446	32.48	0.632	0.47	827
11.0	4.40	4600	68.5505	2.401	0.507	41.51	0.806	0.55	916
11.0	4.40	4500	73.7417	2.418	0.525	42.27	0.779	0.59	828
11.0	4.40	4300	85.2422	2.449	0.546	37.21	0.663	0.64	649
11.0	4.40	4200	91.7339	2.465	0.550	32.57	0.578	0.67	579
11.0	4.40	4100	98.6821	2.479	0.549	26.80	0.462	0.69	477
11.0	4.40	4000	105.8632	2.494	0.546	22.17	0.392	0.71	397
11.0	4.40	3900	113.1294	2.506	0.532	15.18	0.283	0.73	295

[a]Stellar mass (solar units).
[b]Logarithmic luminosity (solar units).
[c]Effective temperature (K).
[d]Period (day).
[e]Logarithmic mean radius (solar units).
[f]Fractional radius variation.
[g]Radial velocity amplitude (Km s^{-1}).
[h]Bolometric amplitude (mag).
[i]Amplitude of logarithmic static gravity.
[j]Effective temperature variation (K).

Table 5. Input parameters and nonlinear observables for Cepheid models of $M = 11\,M_{\odot}$ and solar chemical composition. These models were constructed by adopting the Irwin EOS, the ML relation by Bono et al. (2000), and a coarse zoning across Hydrogen and Helium ionization regions.

M^{a} (1)	$logL^{b}$ (2)	$T_e{}^{c}$ (3)	P^{d} (4)	$\log \overline{R}^{e}$ (5)	$\Delta R/R_{ph}{}^{f}$ (6)	Δu^{g} (7)	$\Delta M_{bol}{}^{h}$ (8)	$\Delta \log g_s{}^{i}$ (9)	$\Delta T_e{}^{j}$ (10)
11.0	4.21	4900	36.9506	2.257	0.282	42.13	0.725	0.26	984
11.0	4.21	4800	39.6741	2.275	0.321	46.38	0.760	0.30	987
11.0	4.21	4600	45.7762	2.309	0.376	44.98	0.648	0.37	835
11.0	4.21	4500	49.0666	2.325	0.396	42.01	0.579	0.40	763
11.0	4.21	4300	56.7848	2.354	0.417	30.17	0.382	0.45	532
11.0	4.21	4200	60.9255	2.368	0.408	18.66	0.216	0.46	309

[a]Stellar mass (solar units).
[b]Logarithmic luminosity (solar units).
[c]Effective temperature (K).
[d]Period (day).
[e]Logarithmic mean radius (solar units).
[f]Fractional radius variation.
[g]Radial velocity amplitude (Km s^{-1}).
[h]Bolometric amplitude (mag).
[i]Amplitude of logarithmic static gravity.
[j]Effective temperature variation (K).

Table 6. Input parameters and nonlinear observables for fundamental Cepheid models with $M = 6.55\,M_{\odot}$ and solar chemical composition. These models were constructed by adopting the Stellingwerf EOS, as well as the ML relation and the zoning used by BCM00.

$M^{\rm a}$ (1)	$logL^{\rm b}$ (2)	$T_e{}^{\rm c}$ (3)	$P^{\rm d}$ (4)	$\log \overline{R}^{\rm e}$ (5)	$\Delta R/R_{ph}{}^{\rm f}$ (6)	$\Delta u^{\rm g}$ (7)	$\Delta M_{bol}{}^{\rm h}$ (8)	$\Delta \log g_s{}^{\rm i}$ (9)	$\Delta T_e{}^{\rm j}$ (10)
6.55	3.48	5600	7.4046	1.767	0.041	16.87	0.267	0.168	300
6.55	3.48	5500	7.8451	1.783	0.057	24.06	0.353	0.255	400
6.55	3.48	5400	8.3426	1.798	0.057	23.61	0.312	0.267	350
6.55	3.48	5350	8.6278	1.806	0.053	21.14	0.262	0.251	300
6.55	3.48	5300	8.8797	1.814	0.047	17.98	0.218	0.228	250
6.55	3.48	5250	9.1559	1.822	0.043	15.55	0.204	0.210	200
6.55	3.48	5200	9.4667	1.830	0.045	17.03	0.217	0.216	250
6.55	3.48	5100	10.139	1.847	0.067	26.58	0.310	0.296	350
6.55	3.48	5000	10.789	1.863	0.086	33.01	0.363	0.348	400

[a]Stellar mass (solar units).
[b]Logarithmic luminosity (solar units).
[c]Effective temperature (K).
[d]Period (day).
[e]Logarithmic mean radius (solar units).
[f]Fractional radius variation.
[g]Radial velocity amplitude (Km s^{-1}).
[h]Bolometric amplitude (mag).
[i]Amplitude of logarithmic static gravity.
[j]Effective temperature variation (K).